FG03-93ER25763
DOE/ER/25163--T3

3.1 APPENDIX I

Homoclinic Orbits and Chaos in a Second-Harmonic Generating Optical Cavity

with Dr. Darryl Holm, *Los Alamos National Laboratory,*
Gregor Kovačič and Ilya Timofeyev, *Rensselaer Polytecnic Institute*

Abstract

We present two large families of Šilnikov-type homoclinic orbits in a two mode-model that describes second-harmonic generation in a passive optical cavity. These families of homoclinic orbits give rise to chaotic dynamics in the model.

Introduction. A standard model of the dynamics of light in a second-harmonic generating passive optical cavity consists of the equations

$$\dot{A}_1 = -i\kappa_1 A_1 + iA_2 A_1^* - \varepsilon\alpha A_1 \tag{1}$$

$$\dot{A}_2 = \frac{i}{2}A_1^2 - \varepsilon(i\kappa_2 + \alpha)A_2 + \varepsilon\gamma_2, \tag{2}$$

where A_1 and A_2 are the slowly-modulated amplitudes of the fundamental color and its second harmonic, κ_1 and κ_2 are the frequency mismatches, $\varepsilon\alpha A_1$ and $\varepsilon\alpha A_2$ are the losses of light in the ring cavity, and $\varepsilon\gamma_2$ is the external pumping of the second-harmonic mode [1, 2, 3, 4]. To derive this model, one must assume that the crystal is short, so that all the spatial effects in it, such as the modulational instability, can safely be neglected [5]. One must also assume that no modes other than a fundamental frequency of the light and its second harmonic can be present in the cavity [1, 4]. Finally, one must assume that the asymmetric crystal in the cavity is of extremely high quality, so that both the pumping and the losses can be taken as relatively small and considered as perturbation terms.

In this paper, we compute two large families of homoclinic orbits that the model (3.1) supports. All these orbits are of Šilnikov type [6, 7, 8, 9, 10], and bring along with them chaotic dynamics arising from a Smale horseshoe construction [11]. Physically, these dynamics should manifest themselves by transient intermittent flickering of light between the fundamental and the second-harmonic colors.

DISCLAIMER

The ideal cavity. When $\varepsilon = 0$, we obtain the equations that describe the ideal cavity without any pumping or losses. They are

$$\dot{A}_1 = -i\kappa_1 A_1 + iA_2 A_1^*, \qquad \dot{A}_2 = \frac{i}{2} A_1^2, \tag{3}$$

and can be derived via formulas $\dot{A}_j = -2i\partial_{A_j} H_0$, $j = 1, 2$, from the Hamiltonian function $H_0 = \frac{1}{2}\kappa_1 |A_1|^2 - \frac{1}{4}\left(A_1^2 A_2^* + A_1^{*2} A_2\right)$. An additional conserved quantity in (3) is the intensity of the light in the cavity, $I = \frac{1}{4}|A_1|^2 + \frac{1}{2}|A_2|^2$.

The canonical transformation $A_1 = \pm\sqrt{2(2I - |a|^2)}e^{-i\frac{\phi}{2}}$, $A_2 = ae^{-i\phi}$ reduces equations (3) into a planar Hamiltonian system for the complex variable a, and a quadrature for the angle ϕ. From this reduced form, we calculate the family of heteroclinic solutions,

$$A_1(t, I, \phi_0) = \pm\sqrt{2\left(2I - \kappa_1^2\right)}\, sech\left(\sqrt{2I - \kappa_1^2}\, t\right) e^{-i\frac{\phi_0}{2}}, \tag{4}$$

$$A_2(t, I, \phi_0) = \left[\kappa_1 + i\sqrt{2I - \kappa_1^2}\, \tanh\left(\sqrt{2I - \kappa_1^2}\, t\right)\right] e^{-i\phi_0}, \tag{5}$$

which connect pairs of equilibria,

$$A_2(-\infty, I, \phi_0) = \left(\kappa_1 - i\sqrt{2I - \kappa_1^2}\right) e^{-i\phi_0}, \quad A_2(\infty, I, \phi_0) = \left(\kappa_1 + i\sqrt{2I - \kappa_1^2}\right) e^{-i\phi_0} \tag{6}$$

that lie in the plane $A_1 = 0$, see Figure 1. (The details of the calculation are similar to but simpler than those in [12].) The difference $\Delta(I)$ in the argument of the variable A_2 after such a heteroclinic excursion is equal to $\Delta(I) = 2\arctan\left(\sqrt{2I - \kappa_1^2}/\kappa_1\right)$.

The pure second harmonic mode. The pure second harmonic mode in the plane $A_1 = 0$ is invariant even for the full system (3.1). Its dynamics are governed by the equation

$$\dot{A}_2 = -\varepsilon(i\kappa_2 + \alpha)A_2 + \varepsilon\gamma_2, \tag{7}$$

which is obtained from (3.1) in this plane. There is a single equilibrium in this plane at

$$A_1 = 0, \qquad A_2 = \frac{\gamma_2}{\alpha + i\kappa_2}, \tag{8}$$

which is, restricted to the $A_1 = 0$ plane, a spiral sink if $\alpha > 0$ and $\kappa_2 \neq 0$. Dynamics in this plane evolve on a slow, $\mathcal{O}(1/\varepsilon)$ time scale.

The n-pulse Melnikov function. For system (3.1), a homoclinic orbit with n pulses consists of two pieces. The first piece is close to n consecutive heteroclinic orbits $(A_1, A_2)(t, \bar{I}, \bar{\phi}_0 - j\Delta(\bar{I}))$, $j = 0, \ldots, n-1$, the first of which is the unstable manifold of the equilibrium point (8), that is, the heteroclinic orbit $(A_1, A_2)(t, \bar{I}, \bar{\phi}_0)$ given by formula (3.1) with

$$A_2(-\infty, \bar{I}, \bar{\phi}_0) = \left(\kappa_1 - i\sqrt{2\bar{I} - \kappa_1^2}\right) e^{-i\bar{\phi}_0} = \frac{\gamma_2}{\alpha + i\kappa_2}. \tag{9}$$

The second piece is close to the trajectory of the system (7) that connects the landing point $A_2(\infty, \bar{I}, \bar{\phi}_0 - (n-1)\Delta(\bar{I}))$ back to the equilibrium (8). The parameters $\bar{I}$ and $\bar{\phi}_0$ in the n pulses are determined by equation (9). The homoclinic orbit only exists if we choose the parameters α, γ_2, κ_1 and κ_2 so that the n-pulse Melnikov function $M_n(\bar{I}, \bar{\phi}_0)$, to be described next, vanishes along the string of heteroclinic orbits $(A_1, A_2)(t, \bar{I}, \bar{\phi}_0), \ldots, (A_1, A_2)(t, \bar{I}, \bar{\phi}_0 - (n-1)\Delta(\bar{I}))$.

The n-pulse Melnikov function [13] is the sum of the ordinary Melnikov functions calculated along each of the heteroclinic pulses (3.1). Here, the ordinary Melnikov function [14, 15] is

$$M(I, \phi_0) = \int_{-\infty}^{\infty} (\nabla H_0 \cdot \mathbf{g})\left(A_1(t, I, \phi_0), A_2(t, I, \phi_0)\right)\, dt,$$

with $\nabla = \left(\partial_{A_1}, \partial_{A_1^*}, \partial_{A_2}, \partial_{A_2^*}\right)$, and $\mathbf{g}$ the $\mathcal{O}(\varepsilon)$ part of the vector field (3.1). (See also the exposition in [16], and the references to original works cited there.) An easy calculation, similar to that in [12], shows that for our model

$$M(I, \phi_0) = \gamma_2 \Im m\left[A_2(-\infty, I, \phi_0) - A_2(\infty, I, \phi_0)\right] + 2\alpha\kappa_1\sqrt{2I - \kappa_1^2},$$

where $\Im m$ denotes the imaginary part of a complex number, so that the n-pulse Melnikov function is given by the expression

$$M_n(I, \phi_0) = \gamma_2 \Im m\left[A_2(-\infty, I, \phi_0) - A_2(\infty, I, \phi_0 - (n-1)\Delta(I))\right] + 2n\alpha\kappa_1\sqrt{2I - \kappa_1^2}. \tag{10}$$

Homoclinic orbits with n-pulses in the shape of a regular n-Gon. We consider homoclinic orbits whose shape is nearly that of a regular n-gon or a regular star with n vertices. By equations (6), adjacent vertices of

such an n-gon or star lie on straight lines tangent to the circle $|A_2|^2 = \kappa_1^2$. Therefore, $I = \bar{I}$ must be chosen so that the angle difference $\Delta(\bar{I})$ satisfies the equation

$$\Delta(\bar{I}) = 2\arctan\frac{\sqrt{2\bar{I}-\kappa_1}}{\kappa_1} = (\kappa_1)\frac{2\pi m}{n} + 2\delta, \tag{11}$$

where $n > 2$ and m are relatively prime integers with $m < n/2$, and δ is a small number.

Equations (9), (10), and (11) imply that if we choose the parameters κ_1, κ_2, and δ, we can compute α and γ_2 so that there exists an n-pulse, Šilnikov type orbit [6, 7, 8, 9, 10] homoclinic to the equilibrium point (8), whose sequence of pulses encircles the origin m times before easing into a spiral of size $2\delta\bar{I}$, which lies close to the plane $A_1 = 0$, and slowly winds back into the equilibrium (8), see Figure 2. Specifically, α and γ_2 are given by the expressions

$$\alpha = (\kappa_1)\frac{2n\kappa_2}{\sin\frac{2\pi m}{n}}\delta^2 + \mathcal{O}(\delta^3), \qquad \gamma_2 = \pm\frac{\kappa_1\kappa_2}{\cos\frac{2\pi m}{n}} + \mathcal{O}(\delta).$$

The first of these equations shows that we must choose the detunings κ_1 and κ_2 to have the same sign in order for these homoclinic orbits to exist in the physical regime $\alpha > 0$.

Apart from the just-described n-pulse homoclinic orbits in which all pulses follow one another in one group or bump, we can also find homoclinic orbits with similar shape in which several bumps, each consisting of n-consecutive pulses, follow one another, being interspersed with slow, spiral-like segments that lie close to the plane $A_1 = 0$. We can form k-bump homoclinic orbits, with each bump containing n pulses, in the following fashion [17]. The first bump of such a homoclinic orbit is close to n consecutive pulses of which the first emanates from the equilibrium (8). There are in fact two such bumps possible; we denote one by $\sigma_1 = +$ and the other by $\sigma_1 = -$, depending on the sign of the real part of the coordinate A_1 at the takeoff. The next segment of this k-bump homoclinic orbit consists of N_1 slow-time revolutions around the equilibrium (8). This segment ends near a curve $A_2(-\infty, I, \Phi(I))$, where the second n-pulse bump takes off. (The existence of this curve easily follows from the simple zero of the Melnikov function at $I = \bar{I}$ and $\phi_0 = \bar{\phi}_0$, and clearly, $\Phi(\bar{I}) = \bar{\phi}_0$.) If the value of I at the takeoff is $I > \bar{I}$, we denote

this takeoff point by $\tau_2 = +$, and if $I < \bar{I}$, we denote this takeoff point by $\tau_2 = -$. The second bump can have the sign $\sigma_2 = +$ or $\sigma_2 = -$ again. This pattern repeats k times, and after the landing of the last bump, the homoclinic orbit spirals into the equilibrium (8). In this way, we can form a homoclinic orbit for every sequence $\sigma_1 N_1 \tau_2 \sigma_2 N_2 \dots \tau_{k-1} \sigma_{k-1} N_{k-1} \tau_k \sigma_k$, where $\sigma_j = \pm$, $\tau_j = \pm$, and $k \leq K_{\max}$. The number $K_{\max}$ depends only on the parameter δ and grows to infinity as δ shrinks to zero. Each such homoclinic orbit is of Šilnikov type, see Figure 3.

Multi-bump homoclinic orbits with an even number of pulses in each bump. We here consider the limit in which the ratio of the detuning κ_1 and the distance $\sqrt{2\bar{I}}$ of the equilibrium point (8) from the origin is very small. In this case, the corresponding phase difference $\Delta(I)$ is close to π for I close to $I = \bar{I}$. We define $\nu(I) = \kappa_1/\sqrt{2I}$, and $\bar{\nu} = \nu(\bar{I})$, and consider the case $\nu(I), \bar{\nu} \ll 1$. Re-computing the $2m$-pulse Melnikov function $M_{2m}(\bar{I}, \bar{\phi}_0) = 0$ along a string of $2m$ consecutive pulses emerging from the equilibrium (8), Taylor-expanding in the small parameter $\bar{\nu}$, and setting $M_{2m}(\bar{I}, \bar{\phi}_0) = 0$ now yields the formula

$$\alpha = m\kappa_2\bar{\nu} + \mathcal{O}(\bar{\nu}^2). \tag{12}$$

For this particular value of α, a Šilnikov-type homoclinic orbit [6, 7, 8, 9, 10] with $2m$ pulses connects the equilibrium point (8) to itself. The pulses of this homoclinic orbit jump between an $\mathcal{O}(\bar{\nu})$-sized neighborhood of the point (8) and an $\mathcal{O}(\bar{\nu})$-sized neighborhood of its antipodal point, until this orbit finally spirals into the point (8). Note that we must again have $\kappa_2\bar{\nu} > 0$, that is $\kappa_1\kappa_2 > 0$, in order that $\alpha > 0$, which is the physical regime.

We now compute the curves along which $2n$-pulse strings of unperturbed heteroclinic orbits takeoff from and land on the A_2-plane for general n. We will use these strings as building blocks in constructing orbits homoclinic to the point (8) with many bumps, each bump consisting of an even, possibly different, number of pulses.

Again re-computing the $2n$-pulse Melnikov function $M_{2n}(I, \phi_0)$, Taylor-expanding in $\nu(I)$, setting $M_{2n}(I, \phi_0) = 0$, assuming $\nu(I) = \bar{\nu} + \mathcal{O}(\bar{\nu}^2)$, and using formula (12), we compute that the takeoff and landing curves in the plane $A_1 = 0$ for the persisting $2n$-pulse strings of heteroclinic orbits (3.1) lie at

$$A_2(-\infty, I, \phi_0(I)) = -(\gamma_2\kappa_2)\left[i\sqrt{2I} + \sqrt{2\bar{I}}(m - 2n)\bar{\nu}\right] + \mathcal{O}\left(\bar{\nu}^2\right), \tag{13}$$

and

$$A_2(\infty, I, \phi_0(I) - (n-1)\Delta(I)) = -(\gamma_2\kappa_2)\left[i\sqrt{2I} + \sqrt{2\bar{I}}(m+2n)\bar{\nu}\right] + \mathcal{O}\left(\bar{\nu}^2\right). \tag{14}$$

In the rest of this discussion, we only consider equations (3.1) in the case when $\gamma_2\kappa_2 < 0$, because the case when $\gamma_2\kappa_2 > 0$ yields almost identical results. We construct a homoclinic orbit that connects the equilibrium (8) at $A_2 = A_2(-\infty, \bar{I}, \bar{\phi}_0) = \sqrt{2\bar{I}}(i - m\bar{\nu}) + \mathcal{O}(\bar{\nu}^2)$ to itself as follows. The first bump of this orbit stays near a string of $2m$ pulses emanating from this equilibrium. Formula (12) shows that this bump exists at some value $\alpha = m\kappa_2\bar{\nu} + \mathcal{O}(\bar{\nu}^2)$. In fact, there exist two symmetric bumps of this kind, which we denote, as in the previous section, by $\sigma_1 = +$ and $\sigma_1 = -$, respectively, depending on the sign of the real part of the coordinate A_1 at the takeoff. This first bump returns to the A_2-plane near the point $A_2 = \sqrt{2\bar{I}}(i+3m\bar{\nu}) + \mathcal{O}(\bar{\nu}^2)$, and the homoclinic orbit continues near this plane along a tight spiral that stays $\mathcal{O}(\bar{\nu}^2)$ close to the circle $|A_2 - \sqrt{2\bar{I}}(i - m\bar{\nu})| = 4m\bar{\nu}$ for N_1 revolutions about the equilibrium point (8).

The second bump of the homoclinic orbit takes off near an intersection point of the circle $|A_2 - \sqrt{2\bar{I}}(i - m\bar{\nu})| = 4m\bar{\nu}$ and one of the lines (13), clearly with $n = n_2 < 3m$ so that this intersection can exist, and consists of $2n_2$ pulses. Since there are two such intersection points, one with $I > \bar{I}$ and one with $I < \bar{I}$, we denote the former by $\tau_2 = +$ and the latter by $\tau_2 = -$. We must also assign the second bump its signature, $\sigma_2 = \pm$, which again depends on the sign of the real part of the coordinate A_2 at the takeoff point of this bump. By formula (14), the landing point on the A_2-plane of the second bump is the reflection of its takeoff point across the line $A_2 = i\lambda + \sqrt{2\bar{I}}m\bar{\nu}$. In other words, this landing point is $\mathcal{O}(\bar{\nu}^2)$ close to the appropriate intersection point of the circle $|A_2 - \sqrt{2\bar{I}}(i + 3m\bar{\nu})| = 4m\bar{\nu}$ and the line (14) with $n = n_2$. The homoclinic orbit then proceeds to wind near the A_2-plane about the equilibrium point (8) along a spiral $\mathcal{O}(\bar{\nu}^2)$ close to the circle $|A_2 - (i - m\bar{\nu})| = R_2\bar{\nu}$. Here, the radius R_2 is computed by a simple application of the Pythagorean theorem to be $R_2 = 4\sqrt{m(m+n_2)}$. The third bump, consisting of $2n_3$ pulses, takes off near an intersection point of the circle $|A_2 - (i - m\bar{\nu})| = R_2\bar{\nu}$ and the line (13), clearly with $n = n_3$. In order for this intersection to exist, we must have $n_3 < m + R_2/2 = m + 2\sqrt{m(m+n_2)}$.

For general j, the j-th bump takes off near the intersection point of the circle $|A_2 - (i - m\bar{\nu})| = R_{j-1}\bar{\nu}$ and the line (13) with $n = n_j$ and lands near the intersection point of the circle $|A_2 - (i + 3m\bar{\nu})| = R_{j-1}\bar{\nu}$ and the line (14) with $n = n_j$. The piece of the spiral that follows this bump lies $\mathcal{O}(\bar{\nu}^2)$ close to the circle $|A_2 - (i - m\bar{\nu})| = R_j\bar{\nu}$, where $R_j = 4\sqrt{m\left(m + \sum_{l=2}^{j} n_l\right)}$. Moreover,

$$n_j < m + \frac{R_{j-1}}{2} = m + 2\sqrt{m\left(m + \sum_{l=2}^{j-1} n_l\right)}. \tag{15}$$

From the discussion we have just concluded it follows that we can form a homoclinic orbit connecting the equilibrium point (8) to itself in the way described above for every sequence of symbols and integers

$$\sigma_1 m N_1 \tau_2 \sigma_2 n_2 N_2 \ldots \tau_{k-1}\sigma_{k-1}n_{k-1}N_{k-1}\tau_k\sigma_k n_k,$$

where $\sigma_j = \pm$, $\tau_j = \pm$, each n_j satisfies the inequality (15), $k \leq K_{\max}$, and the number $K_{\max}$ only depends on the small parameter $\bar{\nu}$ and grows to infinity as $\bar{\nu}$ shrinks to zero, see Figure 4.

Conclusion. We have exhibited two large families of Šilnikov-type homoclinic orbits [6, 7, 8, 9, 10] that are present in the model (3.1). Even though we have assumed that only the second-harmonic mode in the cavity is pumped in this model, it is easy to see that the calculations and results would be nearly identical if the fundamental mode was also pumped by a term of the form $\varepsilon\gamma_1$. Furthermore, well-known arguments show that the homoclinic orbits that we have found imply the presence of a Smale horseshoe return map [11], and thus chaotic dynamics. The orbits generated by the Smale horseshoe map are all unstable, and thus only exhibit transient chaos. However, the presence of homoclinic orbits in the phase space of the model (3.1) is also a likely mechanism responsible for the occurrence of strange attractors seen numerically at $\mathcal{O}(1)$ values of ε in the model [4], and has also been observed experimentally [18]. The numerical investigation of the connection between the homoclinic orbits and this attractor is in progress and will be presented elsewhere.

References

[1] P. D. Drummond, K. J. McNeill, and D. F. Walls, *Opt. Acta*, **27** (1080), 321–335.

[2] P. Mandel and X. G. Wu, *J. Opt. Soc. Am. B*, **3** (1986), 940–948.

[3] V. Zehnle and P. Mandel, *Opt. Comm.*, **66** (1988), 216.

[4] L. A. Lugiato, C. Oldano, C. Fabre, E. Giacobino, and R. J. Horowicz, *Il Nuovo Cimento D*, **10** (1988), 959.

[5] S. Trillo and G. Assanto [1994]. Polarization spatial chaos in second harmonic generation, preprint.

[6] L. P. Šilnikov, *Sov. Math. Dokl.*, **6** (1965), 163.

[7] L. P. Šilnikov, *Sov. Math. Dokl.*, *8* (1967), 102.

[8] L. P. Šilnikov, *Math. USSR Sb.* **10** (1970), 91.

[9] C. Tresser, *Ann. Inst. Henri Poincaré*, **40** (1984), 440.

[10] B. Deng, *J. Diff. Eqns.*, **102** (1993), 305.

[11] S. Smale, in *Differential and Combinatorial Topology*, S. S. Cairns (Ed.), 63–80, Princeton Univ. Press: Princeton, (1963).

[12] G. Kovačič and T. A. Wettergren, *ZAMP*, **47** (1996), 221.

[13] R. Camassa, G. Kovačič, and S.-K. Tin, A Melnikov method for homoclinic orbits with many pulses, submitted to *Arch. Rat. Mech. Anal.*, (1996).

[14] H. Poincaré , *Les Méthodes Nouvelles de la Mécanique Celeste*, 3 vols., Gauthier-Villars: Paris, (1899).

[15] V. K. Melnikov, *Trans. Moscow Math.*, **12** (1963), 1.

[16] S. Wiggins, *Global Bifurcations and Chaos: Analytical methods*, Springer-Verlag: New York, (1988).

[17] T. J. Kaper and G. Kovačič, *Trans. AMS*, **348** (1996), 3835.

[18] C. M. Savage and D. F. Walls, *Opt. Acta*, **30** (1983), 557.

Figure Captions

Figure 1. For fixed ϕ_0, all the heteroclinic solutions (3.1) lie in a plane, and their endpoints (6) all lie on the same straight line tangent to the circle $2I = |A_2|^2 = \kappa_1^2$.

Figure 2. A homoclinic orbit in the shape of a hexagon.

Figure 3. A two-bump homoclinic orbit in the shape of a hexagon.

Figure 4. A homoclinic orbit with two bumps, the first containing two pulses and the second four.

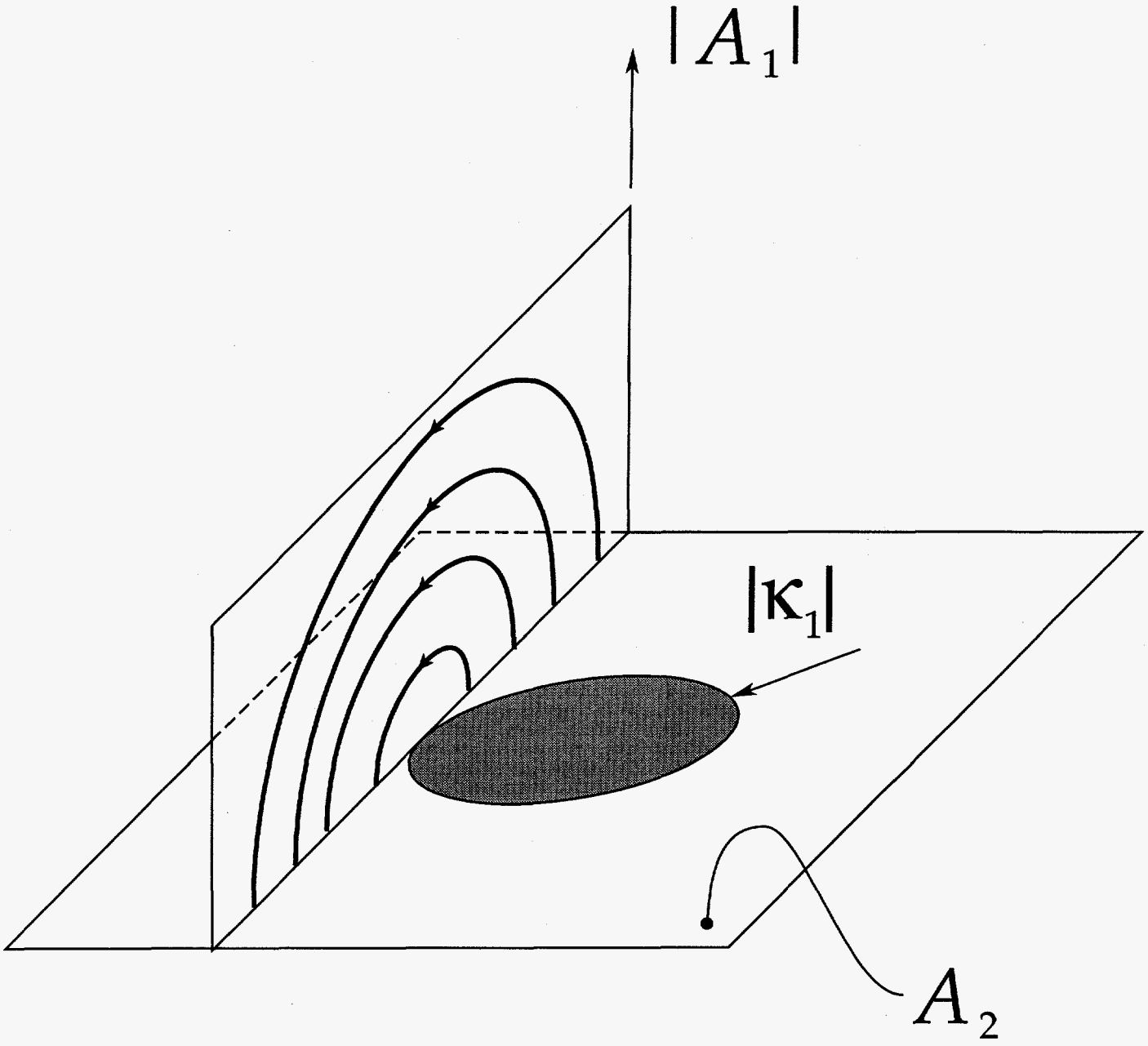

Figure 1

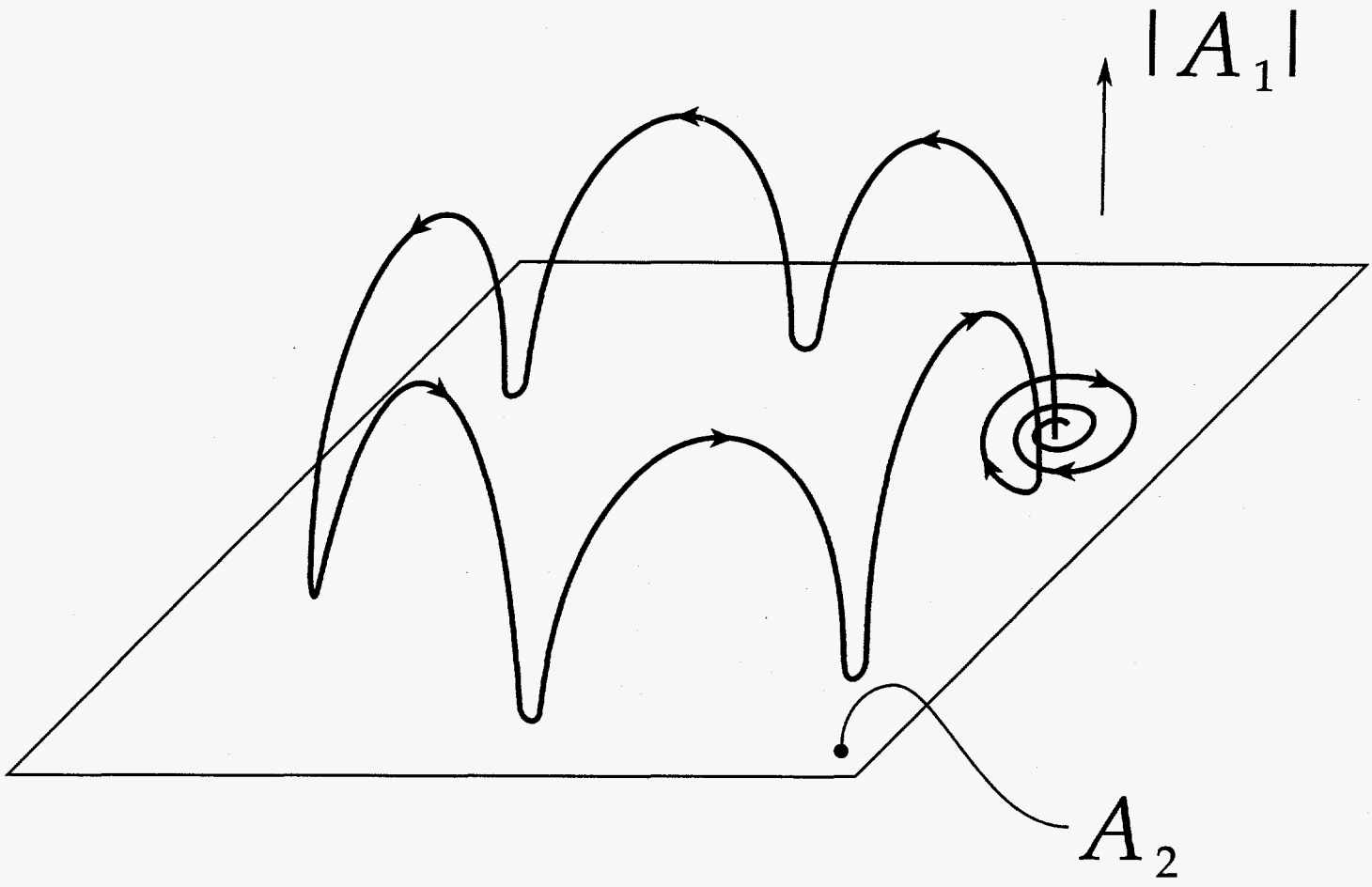

Figure 2

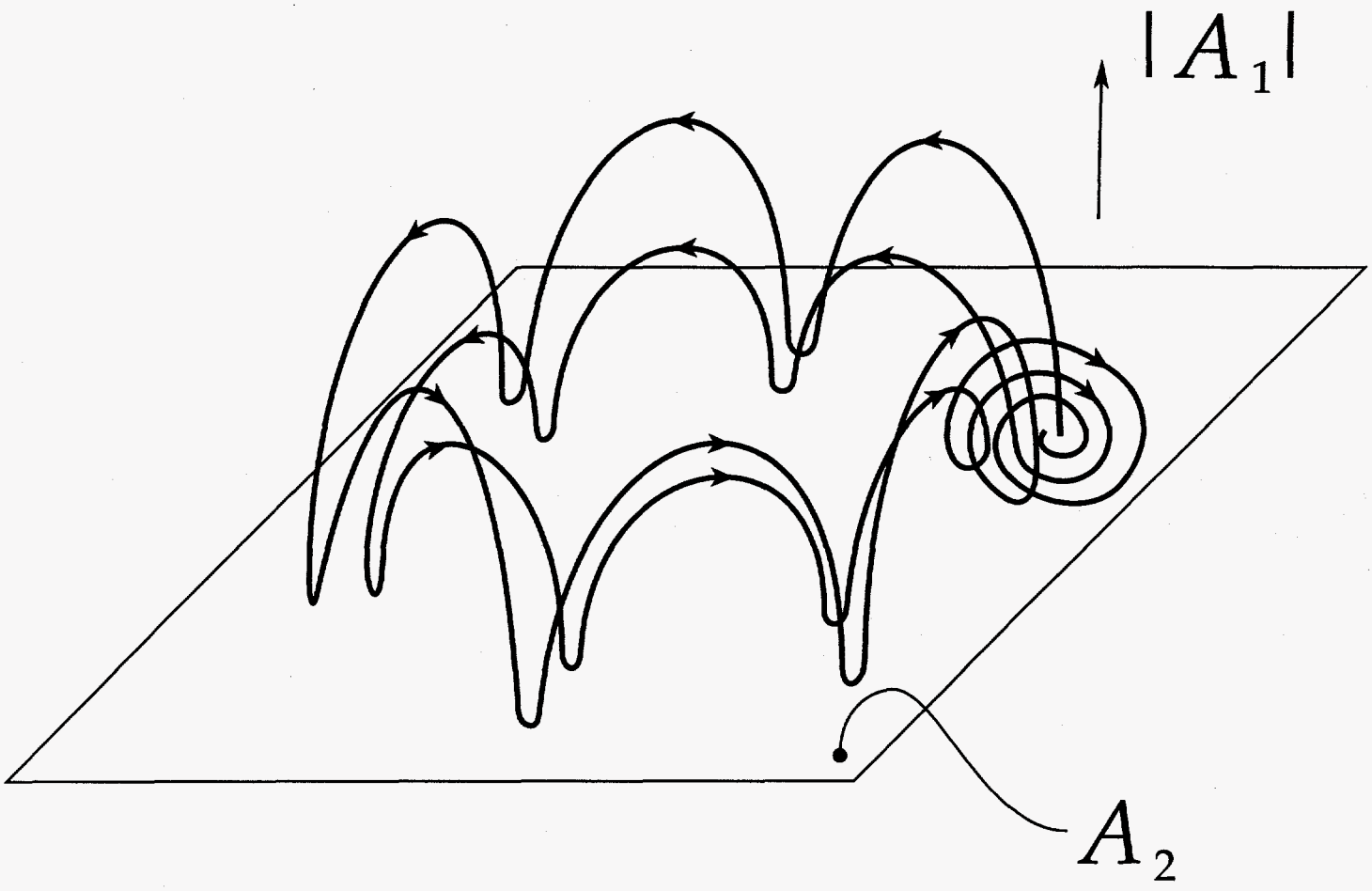

Figure 3

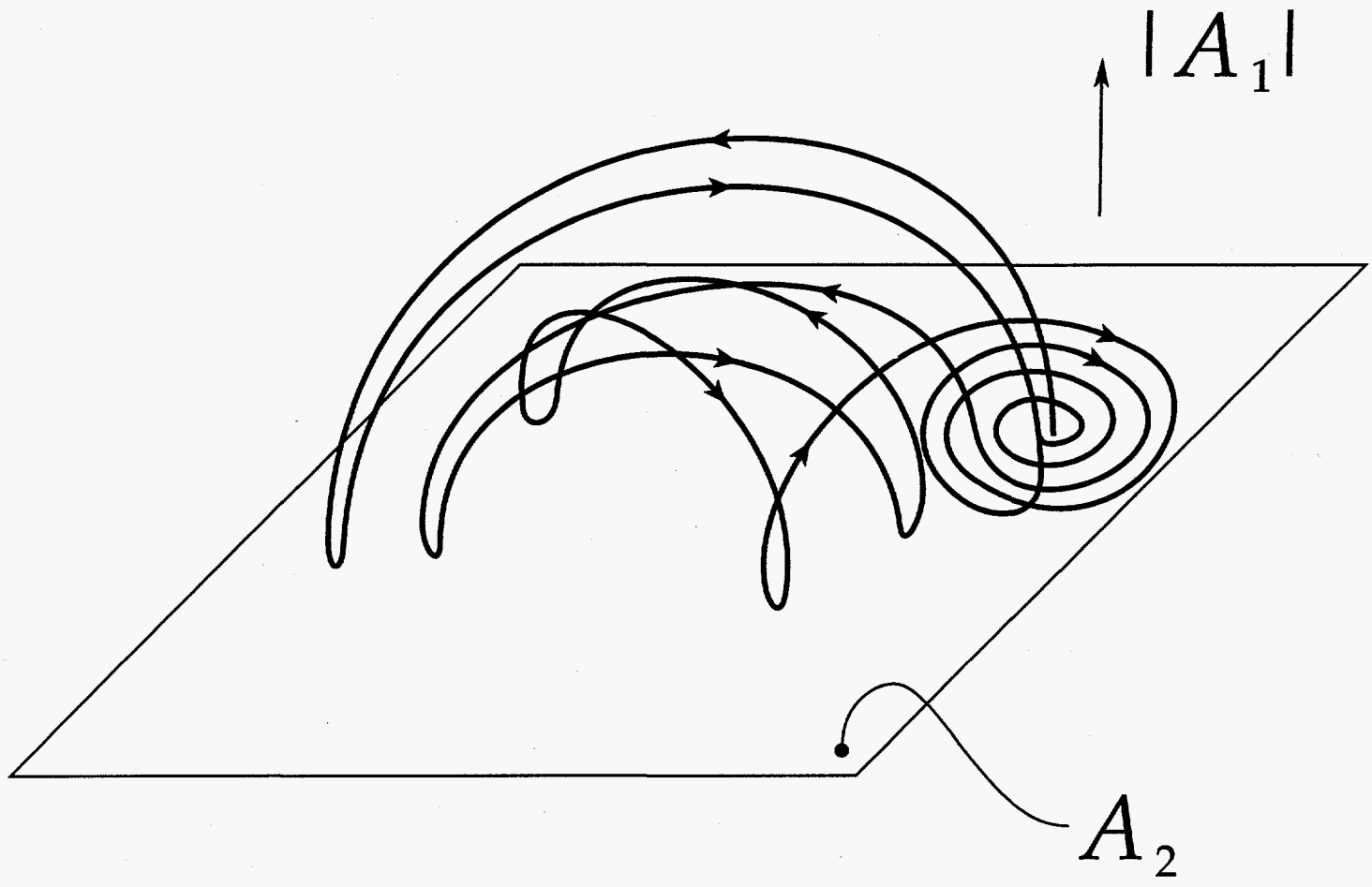

Figure 4